Measurement of residual stresses induced by sequential weld buttering and cladding operations involving a 2.25Cr-1Mo substrate material

Y. Javadi [a, *], J.N. Walsh [b], A. Elrefaey [a], M.J. Roy [a], J.A. Francis [a]

[a] School of Mechanical, Aerospace and Civil Engineering, The University of Manchester, United Kingdom
[b] School of Materials, The University of Manchester, United Kingdom

A B S T R A C T

Dissimilar metal welds are necessary in high-pressure subsea systems and in cases where forged components must be welded to pipelines. F22 (2.25Cr-1Mo) steel is often used in such forged steel components and, since this steel cannot enter service without undergoing post-weld heat treatment (PWHT), the components are usually prepared for field welds through the application of a buttering layer. Furthermore, a weld overlay is deposited for the purpose of mitigating corrosion. This combination of multiple welding tasks and dissimilar materials leads to the possibility of developing substantial residual stresses. This study aims to provide insights to the evolution of residual stresses at each stage of the welding operation. The assessment has been undertaken on laboratory-scale weld mock-ups using the contour method for residual stress measurement, and incremental centre hole drilling. It was found that both buttering and cladding introduce near-yield levels of tensile residual stresses, but that these stresses are successfully relieved upon PWHT.

© 2017 The Authors. Published by Elsevier Ltd. This is an open access article under the CC BY license (http://creativecommons.org/licenses/by/4.0/).

1. Introduction and background

Dissimilar metal welds (DMWs) are used in the construction of many components in the oil and gas industry, including in high-pressure subsea systems. For example, F22 steel forgings are widely used in the manufacturing of pressure retaining valves that need to be welded to steel pipelines (typically API X65 steel). As F22 components are sensitive to hydrogen cracking, post-weld heat treatment (PWHT) is essential in order to relieve the residual stresses and to temper the brittle microstructures that form in the heat affected zone (HAZ) of welds. However, PWHT becomes impractical after components have been joined to pipework and it would also, in general, result in degradation of the material properties of the steel pipeline. A buttering technique, involving the deposition of several layers of low-alloy steel, is therefore usually used so that the buttered F22 steel can be heat treated before the closure weld (i.e. to adjoining pipework) is carried out.

The residual stresses that are introduced by welding can affect the structural integrity of safety-critical components [1,2].

Although a weld-buttered component undergoes PWHT to reduce residual stresses, subsequent thermal cycles associated with a closure weld will contribute to an increase in residual stresses at the interface between the forging steel and the weld buttering layer [3—6]. In the oil and gas industry, these components are also clad on internal surfaces in order to protect the underlying steel from corrosive environments [7—9]. While PWHT takes place after the cladding operation, the presence of dissimilar materials can contribute to the generation of residual stresses if further thermal cycles are applied, particularly near to the interfaces between these materials [10—12].

In recent years, there has been interest in increasing the allowable operating pressures and temperatures for subsea systems. Under such circumstances, materials would be utilised closer to their operating limits, and it becomes increasingly important to quantify the levels of residual stress in critical locations such as dissimilar metal welds. However, the combination of complex geometries, dissimilar materials, and relatively thick components tends to restrict our ability to measure residual stresses on components that are in service. For these reasons, increased reliance is placed on numerical models as a means of predicting residual stresses. However, such models need to be validated by comparing

* Corresponding author.
  E-mail address: yashar.javadi@manchester.ac.uk (Y. Javadi).

numerical predictions with the residual stresses that are measured on well-characterised benchmark specimens [13,14].

This experimental study aims to provide insights to the generation of residual stresses in a complex dissimilar metal weld, i.e. one in which a large F22 forged component is clad and weld-buttered in preparation for welding to a pipe. To this end, welding protocols were developed for buttering low-alloy steel (LAS) onto F22 parent material, and for internal cladding with Inconel 625 alloy.

Dissimilar metal welds of this type are normally executed on pipes in the form of girth welds. However, in this study it was not feasible to apply the relevant combination of welding processes, within a controlled laboratory environment, to girth welds that had a diameter and wall thickness that were representative of components that are used in subsea installations. Furthermore, the authors aspired to employ the contour method [15] to measure residual stresses in this work. When planning the work the authors formed the view that, while the contour method has recently been applied with success to girth welds [16–18], the additional complexities associated with substantially dissimilar material properties, and the particular manufacturing sequence, would have added significantly to the challenges and uncertainties associated with the measurements. Thus, a flat plate geometry was chosen, noting that the contour method has long been established for specimens with this configuration. Moreover, the design of the specimens was chosen specifically so that residual stresses could be measured using the contour method, which has been recently used for the measurement of residual stress in welded components in ultra-thick ferritic steel [19].

It is clearly important to note that the development of residual stresses in plate specimens will not match the development of stresses in a tubular component, as the nature of the restraint during welding will differ significantly. However, the ultimate goal with this work was to design weld mock-ups that could serve as (benchmark) validation cases for the application of finite-element models. Such models could subsequently be used to predict residual stresses in full-scale dissimilar metal welds in deep water subsea installations, which would normally be too expensive to subject to destructive residual stress measurements. In the hope of maximising the utility of this work, the authors endeavoured to be as faithful as possible to industrial practice when the specimens were manufactured.

The specific combination of materials that has been employed in this work, and the manufacturing sequence, do not appear to have been investigated in the literature. Furthermore, there is a paucity of studies that have employed contour method measurements to dissimilar materials. However, the manufacturing sequence applied in this work mirrors that which is employed for a standard 6″ subsea valve and, at each stage in the manufacturing sequence, a sample was extracted and characterised (Fig. 1). The contour method was employed to map longitudinal residual stresses on a plane that was orientated transversely to the welding direction and, for the two stages in the manufacturing sequence that are described in this article, the results were supplemented by incremental hole drilling measurements, which also provide values for the transverse residual stresses.

2. Experimental methodology

2.1. Manufacture of test pieces

Two nominally identical specimens were manufactured with the geometry and dimensions as shown in Fig. 2. Plates were machined from F22 forging steel to a thickness of 30 mm to provide material that would be representative of a forged component. The F22 steel plates were machined so that they included a weld bevel angle of 30°, and then subsequently placed on a 20 mm thick backing plate, which was machined from S275 steel. A buttering layer was deposited onto the machined bevel on the F22 steel plate, as well as on to the backing plate, using a low alloy steel (LAS) filler metal, OP-121-TT flux, and the submerged arc welding (SAW) process. The nominal chemical compositions for the base material, filler material, backing plate and welding flux are given in Table 1, and the material properties are summarised in Table 2. The deposition sequence is illustrated schematically in Fig. 3.

In the case of a real engineering component, the F22 steel would likely be in the form of a nozzle (i.e. a solid body of revolution), and the backing plate might take the form of a ring that would be used to support the buttering layer during deposition. After the buttering process was completed, the backing plate was machined off to provide a pocket for the deposition of an inconel 625 weld overlay. This overlay is intended to simulate the internal cladding of nozzles and pipes for the purpose of imparting corrosion resistance. Gas-tungsten arc welding (GTAW) was used to apply two layers of metal to the back face of the sample. The deposition sequence is illustrated schematically in Fig. 4. After the buttering and cladding operations were completed, one of the samples was sent for PWHT while the other was retained in the as-welded condition. The PWHT procedure involved the specimens being held in air at 630 °C for 7 h 15 min, followed by air cooling. The welding parameters for the buttering (SAW) and cladding (GTAW) are listed in Table 3.

It is worth mentioning that in the case of components such as nozzles and pipes, the relative stiffness of these components is greater than that for plates, i.e. the geometry of these components would assist in reducing the effects of weld distortion. Plates, however, will distort significantly if a large number of weld passes is deposited onto one side of the specimen. Significant levels of distortion would also influence the development of residual stresses in the component, as well as the subsequent measurement of residual stresses. As can be seen in Fig. 2, strong backs were attached by welding to the back surface of the weld mock-ups. These strong backs served to provide increased stiffness and to reduce the extent of distortion during welding. The specimens were also fitted with webs for the same purpose. These webs were welded to both the strong backs and the back surface of the weld mock-up. However, the webs could not traverse the entire length of the specimen in the welding direction as this would have presented significant difficulties for the cutting stage when applying the contour method for residual stress measurements.

2.2. Contour method

The contour method is a three-step process in which the component is firstly cut to relieve the stresses acting normal to the cut surface. In the second step, the distortions generated on the cut surface (owing to the relaxation of stress) are measured to provide the input boundary conditions for a finite element (FE) model. The third step could comprise an elastic finite element analysis, in which the deformed surface is forced (in a virtual sense) to be flat, and the stresses required to do so are calculated. These calculated stresses are then taken to be the negative of the residual stress distribution that was acting in a direction normal to the cut surface, prior to the cut being made [20].

Whilst current best practice for performing this third step remains an FE analysis, completely analytical approaches have been validated for an aluminium alloy 2024-T351 specimen that was welded using variable polarity plasma arc welding [21]. Validation of these analytical approaches was carried out via a conventional contour method (FE based) analysis and via neutron diffraction [22]. However, analytical techniques were not employed in this
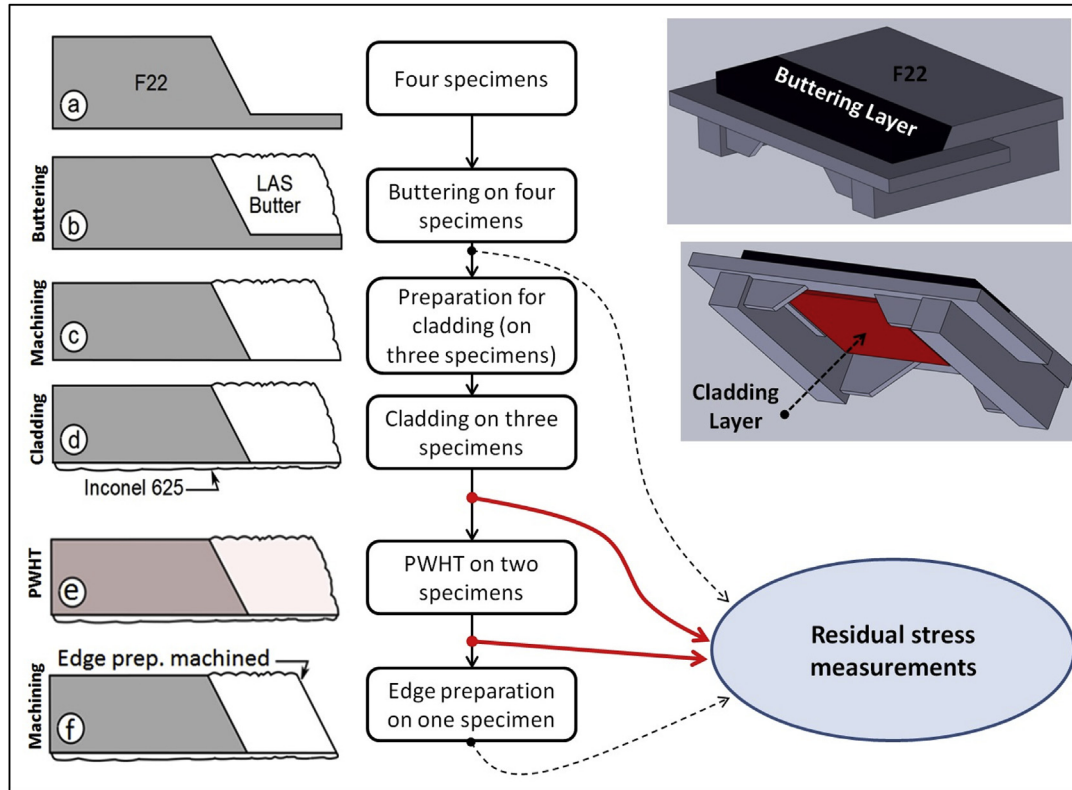
Fig. 1. Representation of the manufacturing sequence for the flat plate specimens. The most comprehensive residual stress measurements were carried out at stages in the manufacturing sequence that are called out by bold red arrows. These measurements form the basis of this article. (For interpretation of the references to colour in this figure legend, the reader is referred to the web version of this article.)
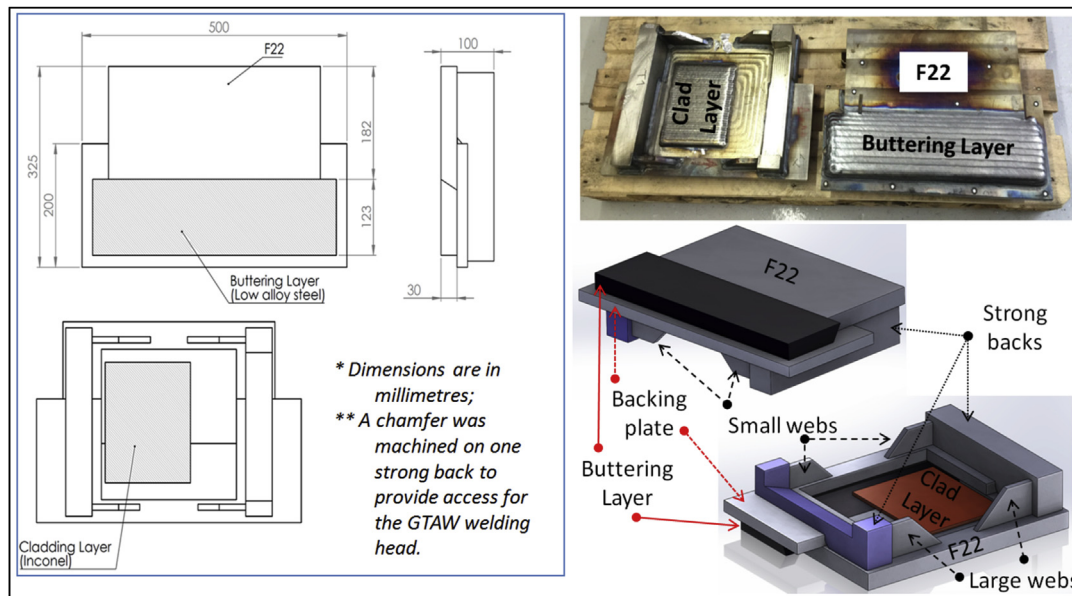

Fig. 2. Specimen geometry and dimensions (all dimensions in millimetres).

work due to the flexibility offered by an FE-based approach, giving particular consideration to the differences in the elastic properties of the materials that were employed.

The contour method analysis commenced with a cutting step carried out by electric discharge machining (EDM) in order to minimise the introduction of stresses to the part during cutting.

The use of self-restraint, through the drilling of pilot holes close to the edges of the surface to be cut, on the cutting plane, prior to cutting, is recommended [15,17,20] in order to change the geometry of the cut from that of an edge crack to a centre crack, thus reducing the likelihood of plasticity. These pilot holes were produced by an EDM operation at the positions shown in Fig. 5.

Table 1
Nominal chemical compositions for the base material, filler materials, backing plate and welding flux (wt.-%).

	F22 base material		Filler materials					S275 backing plate	Welding flux[h]
			GTAW			SAW			
	Cert.[a]	Meas.[b]	Cert.[c]	Meas.I[d]	Meas.II[e]	Cert.[f]	Meas.[g]		
C	0.14	0.152	0.013	0.024	0.024	0.07	0.069	0.25 max	0.07
Mn	0.57	0.49	0.01	0.02	0.06	1.5	1.49	1.6 max	1.3
Si	0.19	0.24	0.07	0.08	0.08	0.3	0.16	0.05 max	0.2
P	0.005	0.007	0.003	<0.005	<0.005		0.018	0.04 max	
S	0.002	0.004	0.001	0.002	0.003		0.006	0.05 max	
Cu	0.1	0.19	0.01	<0.02	<0.02		0.09		
Ni	0.48	0.16	64.5	63.55	62.59	1	0.84		
Cr	2.5	2.36	22.4	22.21	21.21		0.13		
Mo	1.05	1.03	9	9.03	8.7	0.5	0.5		0.5
V	0.004	<0.05					<0.05		
Ti	0.002	<0.05	0.18	0.17	0.17		0.38		
Al	0.019	<0.05	0.09	0.09	0.08		<0.05		
N	0.006	0.011					0.007		
Nb	0.006	<0.05	3.48	3.41	3.28		<0.05		
Sn	0.007	<0.05					<0.05		
Ca	0.001	<0.05					<0.05		
Fe	94.9	95.5	0.3	1.32	3.7		96.63		

[a] Based on certification provided by the manufacturer of F22 steel.
[b] Chemical composition measured for F22 steel base material after buttering and cladding.
[c] Based on certification provided by the manufacturer of ERNiCrMo-3 filler wire.
[d] Chemical composition measured in the first layer of cladding overlay.
[e] Chemical composition measured in the second layer of cladding overlay.
[f] Based on certification provided by the manufacturer of OE-S3 NiMo 1 filler wire.
[g] Chemical composition measured in the buttering layer, away from base material and backing plate.
[h] Nominal all-weld-metal chemical composition when OP 121 TT flux is used in combination with OE-S3 NiMo 1 filler wire, as quoted by manufacturer.

Table 2
Material properties.

	F22 base material[a]	Low alloy buttering[b]	Inconel cladding[c]
Young's modulus (GPa)	206	205	207
Poisson's ratio	0.301	0.29	0.29
Yield stress (MPa)	598 ± 2	540	452
UTS (MPa)	719 ± 2	650–750	760
Elongation (%)	23 ± 2	20	42
Thermal expansion coefficient (10^{-6} mm/mm/°C)	14.4–16.2	14.4–15	11.5–12

[a] The mechanical properties are based on the results of five tensile tests.
[b] The mechanical properties are based on certification provided by the manufacturer of OE-S3 NiMo 1 filler wire.
[c] The mechanical properties are based on certification provided by the manufacturer of ERNiCrMo-3 filler wire.

In terms of the location of pilot holes, the most common practice is to choose locations near to the edges of the specimen and/or cutting plane, since this maximises the extent of the contour cut and, for many specimen geometries, it also places the pilot holes away from regions sustaining high levels of stress. In the case of this work, however, the number of weld passes was extremely large and the levels of internal stress were also large across the entire specimen width. In a trial measurement on the specimen geometry that was used in this work, pilot holes were initially placed at a distance of 10 mm from either edge of the specimen. However, it was found that this choice led to excessive deformation in the remaining ligaments of material during the EDM cutting operation and consequently, to excessive movement of the cut surface as cutting proceeded.

Excessive deformation during cutting would lead to one of the underpinning assumptions for the contour method being violated, i.e. that the surface of the cut was perfectly planar prior to the cutting step. Accordingly, the location of one pilot hole was moved so that it was further from the specimen edge, as shown in Fig. 5. Although the new location for the pilot hole coincided with both the buttering layer and the cladding overlay, it was still a significant distance from the interface between the F22 steel and the buttering layer, which is a location of primary interest from a structural

integrity standpoint. It was assumed that the specimen could be cut in a piecewise manner, as shown in Fig. 5, and that the resulting contours could be stitched together to reconstruct the original residual stress distribution.

The contour cut was performed between the pilot holes, with the ligaments on either side of the holes taking up the stresses that were relieved on the cutting plane during the cutting operation. Errors introduced during cutting depend largely on how the sample is clamped in the EDM machine; hence clamping is a primary consideration for producing a good contour cut and obtaining data of high quality. External restraint was applied through using a combination of normal and G-clamps, as shown in Fig. 6a, to restrain the plate at its four corners. Various studies [15,17] have shown that applying constraint close to the cutting plane is an effective means of reducing, or eliminating, plasticity during cutting. In this work, restraint was applied using a customised rig, which is shown in Fig. 6b.

The set-up included bolts with ball-jointed ends to apply restraint close to the cutting line, particularly for mock-ups with an uneven surface. The rig consisted of 4 bars, which were located above and below the plate on either side of the cutting line, from which flat-headed screws spaced at 10 mm protruded to make contact with the surface of the specimen over an area with a
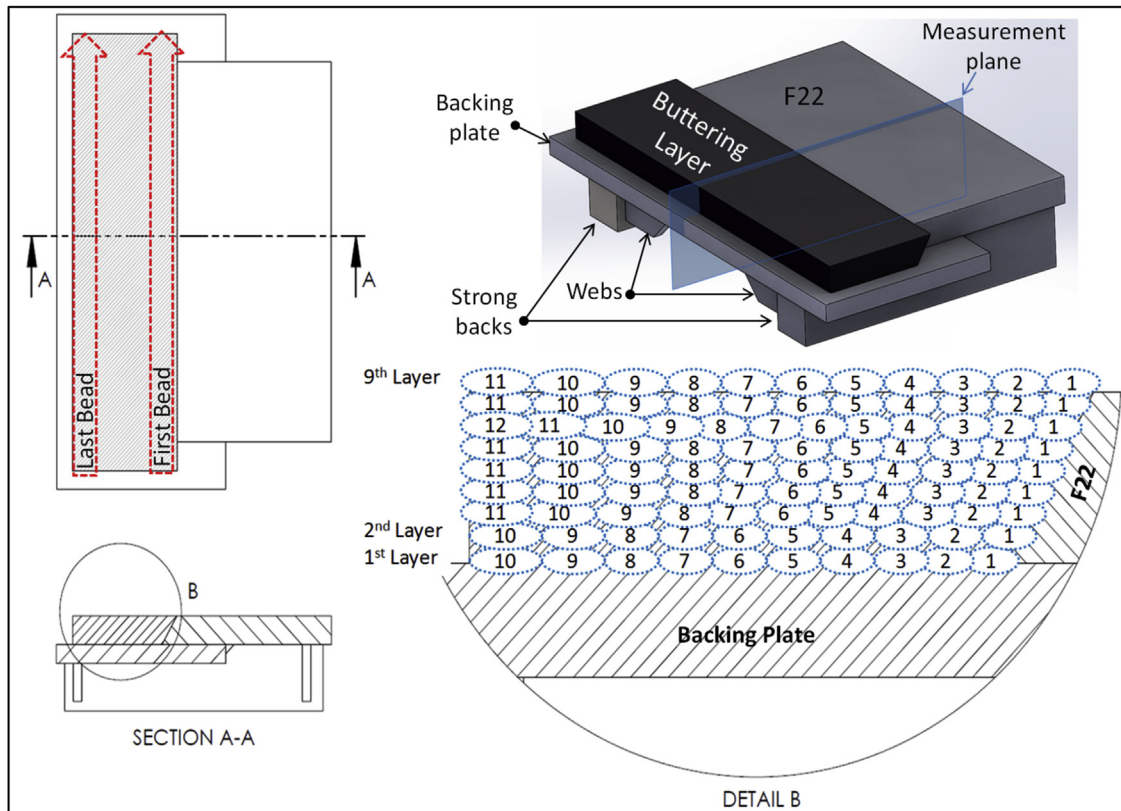
Fig. 3. Deposition sequence for buttering process, which was carried out by submerged arc welding.
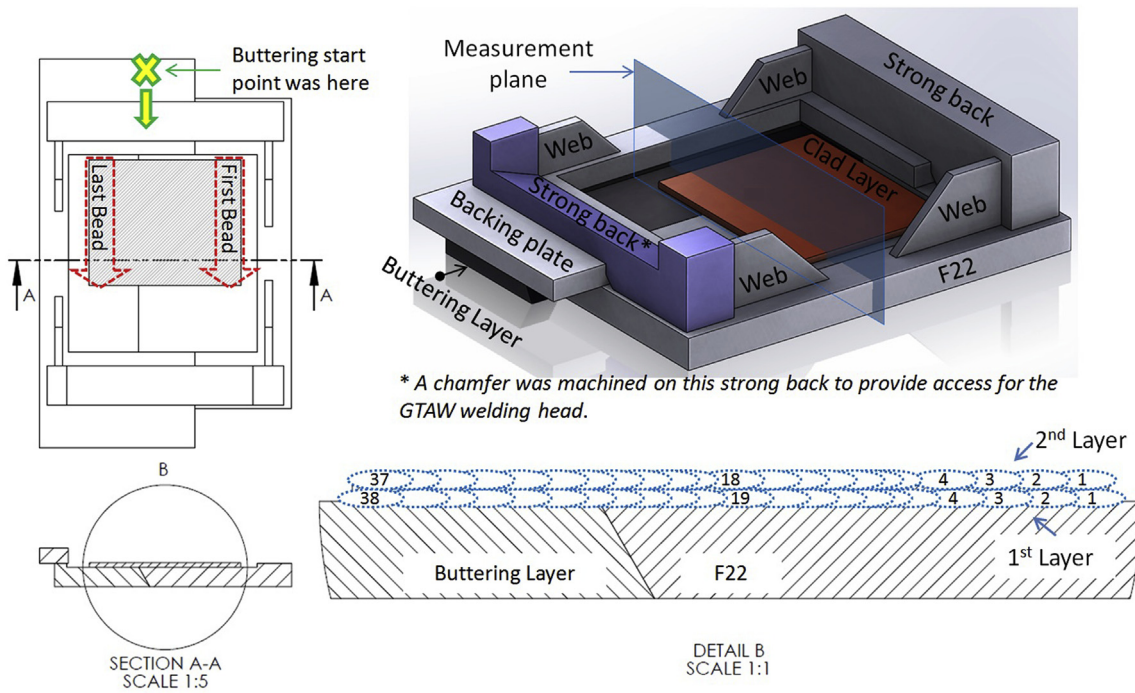

Fig. 4. Deposition sequence for cladding process, which was carried out by GTAW.

diameter of 8 mm. It should be noted that the specimens in this study had a complicated geometry in comparison with samples typically used in contour method measurements. Plasticity is probably the most significant source of error during the cut; it occurs when the stress at the cutting tip is larger than the yield stress of the material. The cut surface that was achieved in the AW

Table 3
Welding parameters employed in buttering and cladding operations.

Buttering process	Number of layers	9
	Number of weld beads in each layer	(Layer 1 and 2: 10 beads); (Layer 3−6 and 8−9: 11 beads); (Layer 7: 12 beads)
	Thickness	30-31 mm for 9 layers in total (buttering thickness)
	Welding Voltage	27 V
	Welding Current	350 A
	Welding Speed	240 mm/min
	Material	Wire: OE-S3 NiMo 1 (EN 756; AWS − SFA 5.23-EG)
		Flux: OP 121 TT (EN 760 − SA FB 1 55 AC H5)
	Filler wire diameter	2.4 mm
	Preheating temperature	180-220 °C
Cladding process	Number of layers	2
	Number of weld beads in each layer	(1st Layer: 38 beads); (2nd Layer: 37 beads)
	Thickness	6 mm for 2 layers in total (cladding thickness)
	Welding Voltage	12 V
	Welding Current	250 A
	Welding Speed	140 mm/min
	Wire feed speed	2000 mm/min
	Filler material	ERNiCrMo-3 (EN ISO 18274; A5.14/ASME SFA 5.15)
	Filler wire diameter	1.2 mm
	Shielding Gas	Pure Argon
	Preheating temperature	150 - 180 °C
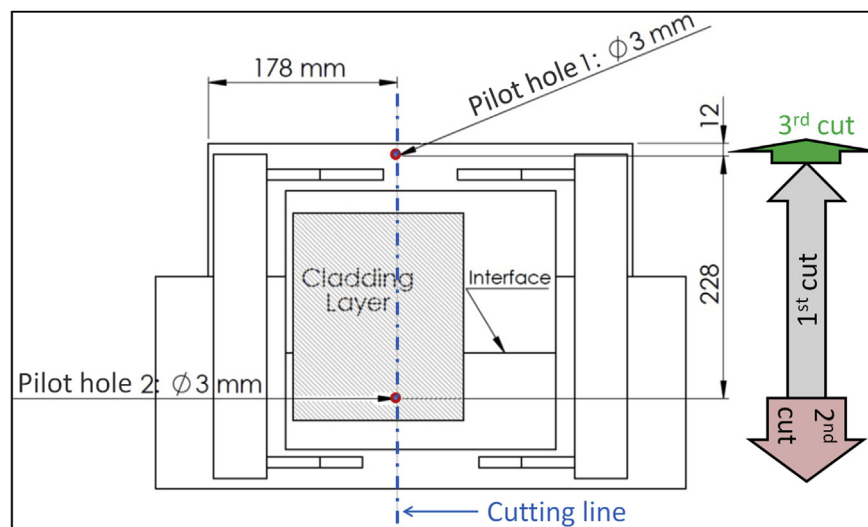
Fig. 5. Positions of the holes produced by EDM to enable self-restraint during the cutting operation.

sample is shown in Fig. 6c.

Following the cutting process, the deformations on the cut surface resulting from the relaxation of stresses were measured using a coordinate measurement machine (CMM). Points were measured with the spacing varying from 0.5 mm in the vicinity of a polyline describing the boundaries between the different alloys (e.g. either between the buttering layer and the F22 steel, or between the cladding overlay and F22 steel/buttering layer) to 1 mm further away from these areas. These spacings were chosen as a compromise between the time taken to measure one surface, and having as dense a measurement point cloud as possible. Surface alignment, averaging and spline fitting were performed using Matlab®.

The raw measured surfaces for the AW sample are shown in Fig. 7. In addition to points on the top surface, the outline of each part was also measured as a closed contour, as can be seen in Fig. 8. There are two principal sources of error in surface measurements, which lead to uncertainties in stress determination; these are displacement errors such as high frequency noise from the surface roughness, and measurement errors, which depend on the

measurement spacing. Since the surface roughness is determined by the peculiarities of the part to be cut, the chosen measurement spacing should depend on a realistic assessment of the resolution that one can expect to achieve.

The surfaces must be fitted to mitigate the effects of noise in the data. Standard practice is to fit a bi-variate spline function, with a "spline" comprising a number of different polynomial functions which together describe a more complex curve, with each polynomial describing a small portion of the curve very accurately between locations, known as knots, where the polynomials join. Thus, with a small number of parameters, the polynomial coefficients and the knot locations, the surface can be fitted in a least-squares minimisation process. Since it is desirable in the fitting process to "smooth out" noise, it is difficult to estimate the goodness of the spline fit. The least-squares fit result will continue to improve as the spline incorporates more data points, even if the new data points are noisy. Overfitting will result in noisy values being incorporated into the surface and underfitting will smooth out valuable information. How much smoothing occurs is determined by the knot spacing of the splines − i.e. the distance over which one polynomial
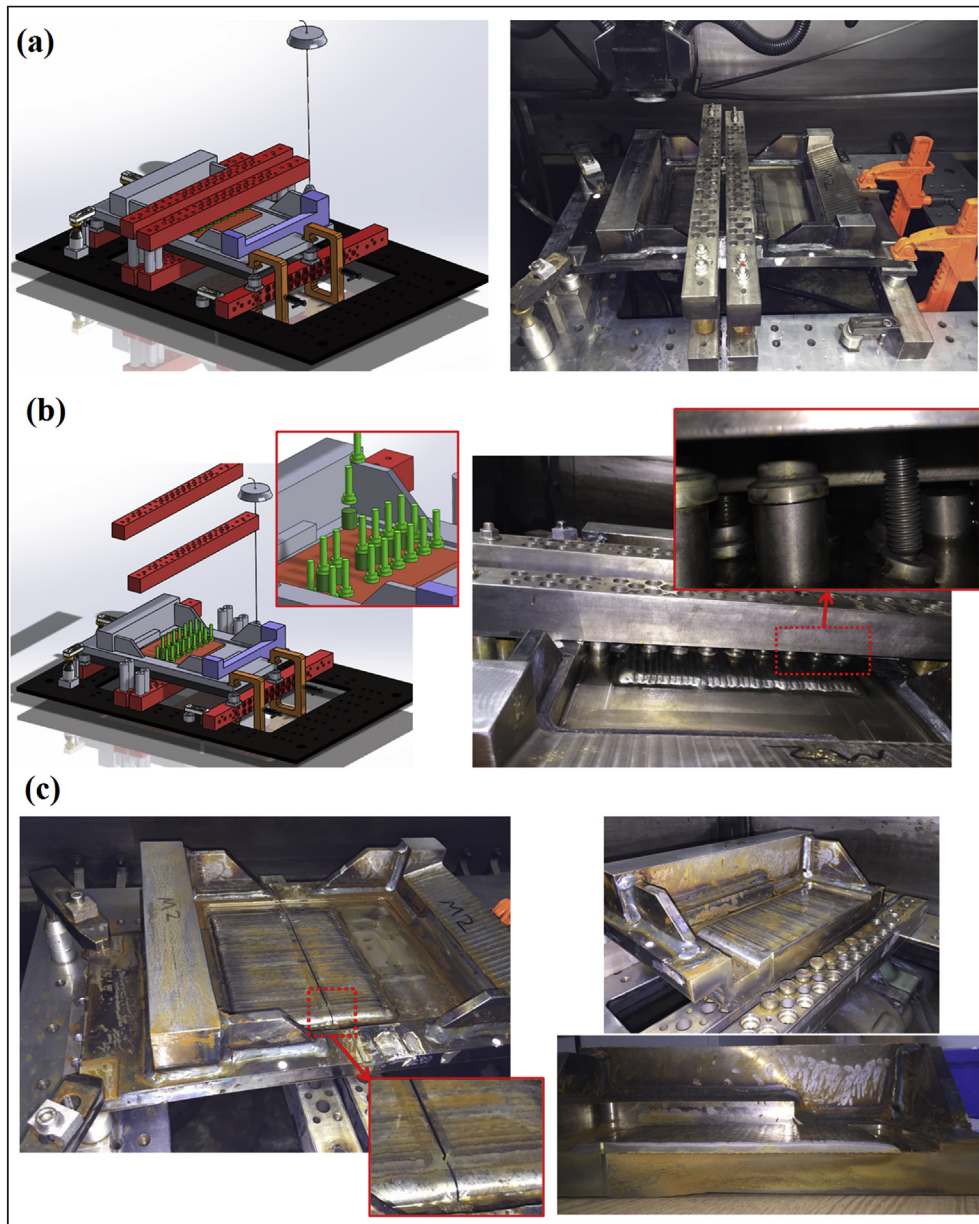
Fig. 6. Set-up for restraint of test pieces during EDM cutting (a: simple clamping with G-clamps; b: customised restraint rig including flat-headed screws as well as bolts with ball-jointed ends, which can accommodate weld mock-ups with an uneven surface; c: cut surface).
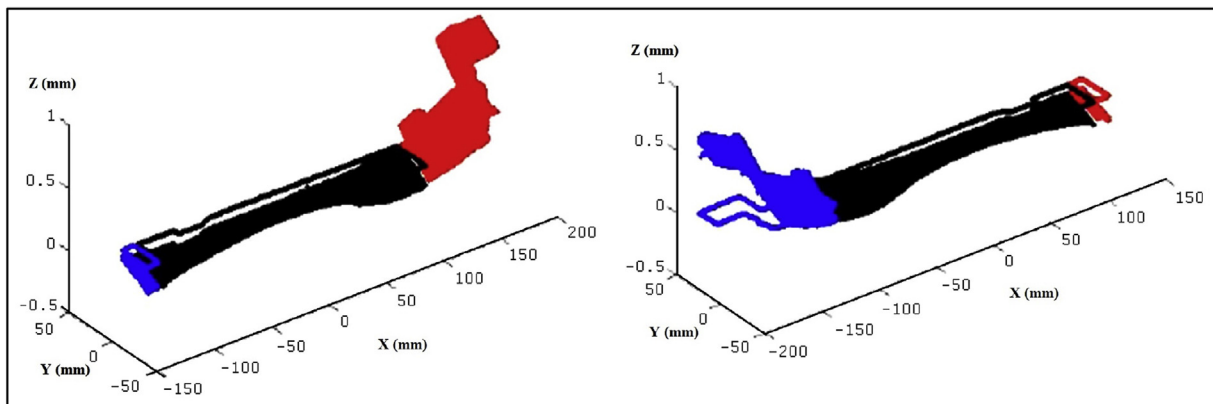

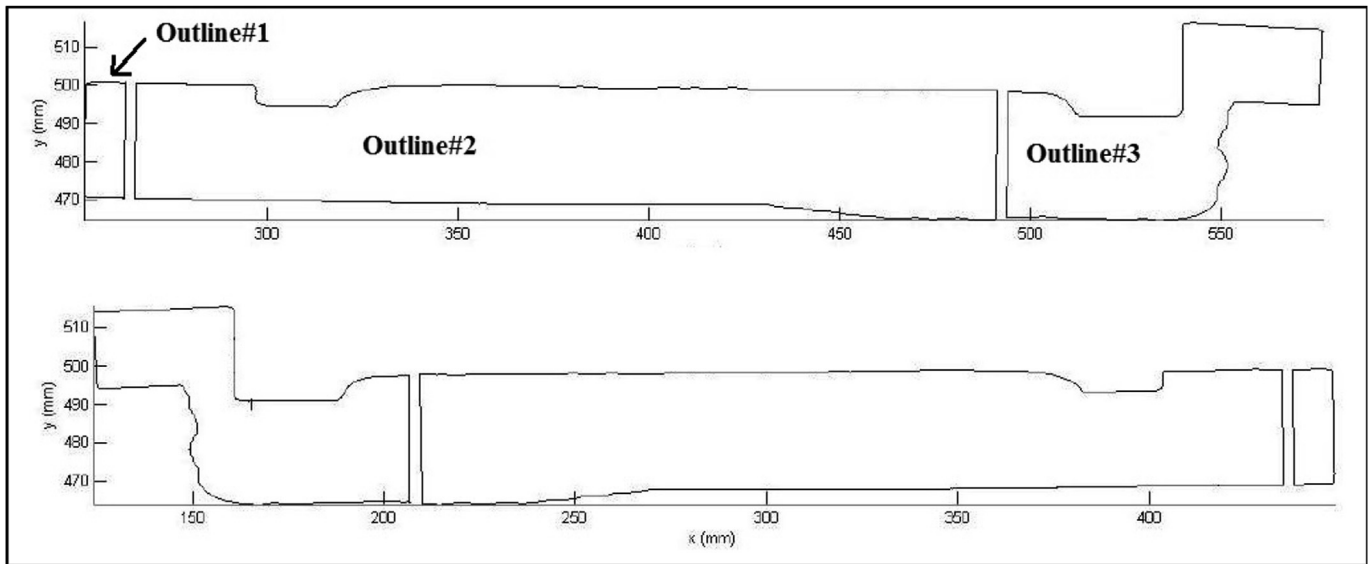**Fig. 7.** Raw measured surfaces for the AW sample.

Fig. 8. Measured surface outlines for the AW sample.

must fit the surface.

Given a minimum measurement spacing of 0.5 mm as was used here, the smallest feasible knot spacing would cover the distance spanned by 3 data points: 1 mm. It is somewhat harder to judge the maximum feasible knot spacing; here we considered the features that defined the samples - the weld beads in the buttering and cladding layers. The buttering beads were approximately 9 mm wide with 4–5 mm overlap, while the cladding beads were approximately 6 mm wide with 1–2 mm overlap. We assumed that the surface deformation would vary continuously within one bead (excluding contributions from noise) and therefore that the maximum range for one spline should be one weld bead width or ∼ 5 mm. This determined our potential range of knot spacings to be between 1 and 5 mm. It is hard to judge how the choice of knot spacing will impact on the estimated stresses without calculating the stresses for a variety of knot spacings and visually inspecting the results. In the case of the AW sample, the stresses were calculated for splines with knot spacings of 1, 2, 3, 4, 5, 6 and 7 mm. The statistics for these surface fits, in terms of root-mean-square error between the measured and fitted surfaces, are shown in Fig. 9. The corresponding stress profiles are shown in Fig. 10. A knot spacing of 4 mm was chosen for the final analysis, as this gave at least one spline per weld bead in the cladding layer, and it led to a minimum of noise in the final estimates for stress.

The finite element analyses were performed using ABAQUS with tetrahedral quadratic C3D10 elements; a typical mesh is shown in Fig. 11. Displacement boundary conditions were applied to the cut surface. In each case, the fitted surface was evaluated at the node locations of the finite element mesh and the displacements were applied as boundary conditions, together with three additional constraints to prevent rigid body motion. These additional constraints were imposed at single nodes on the edges of the pilot holes. The output of the FE analysis was the estimates for stress at the integration points on the cut surface. Due to the high degree of deformation seen in the as welded (AW) samples, a second analysis was also performed in which a yield stress was specified and, as deformation progressed and the stress in the sample reached the yield stress, the sample was allowed to deform plastically. It is recognised, however, that this approach contravenes the principle of elastic superposition on which the contour method is founded,
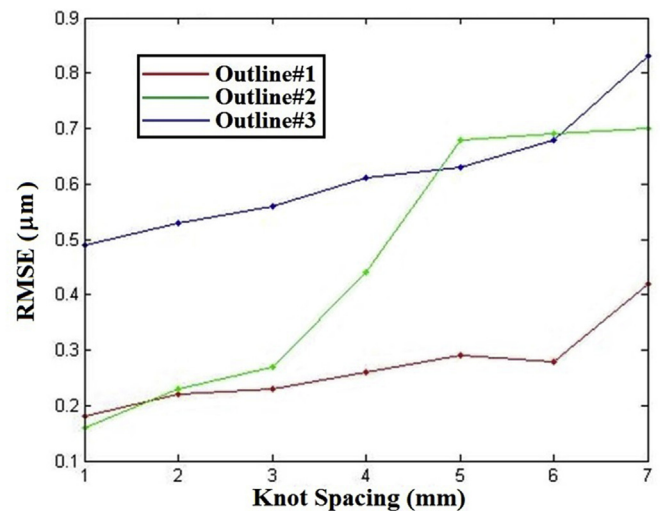

Fig. 9. Root Mean Square Error (RMSE) between fitted and measured surfaces for different knot spacings (Outline numbers are shown in Fig. 8).

and this second analysis was carried out solely to assist in identifying locations that were likely to be subject to errors associated with cutting-induced plasticity. Material properties were assigned using image correlation between the mesh and the macrograph presented in Fig. 12, which shows the fusion boundaries for the buttering layer and cladding overlay.

2.3. Incremental hole-drilling method

Residual stresses were measured using the incremental hole-drilling method as shown in Fig. 13. As incremental hole drilling is a standardised technique [23], this method was used in order to check for consistency with the residual stresses measured by the contour method. Incremental hole-drilling was implemented on both the AW and PWHT samples at nine and six locations, respectively. This semi-destructive technique measured the strain
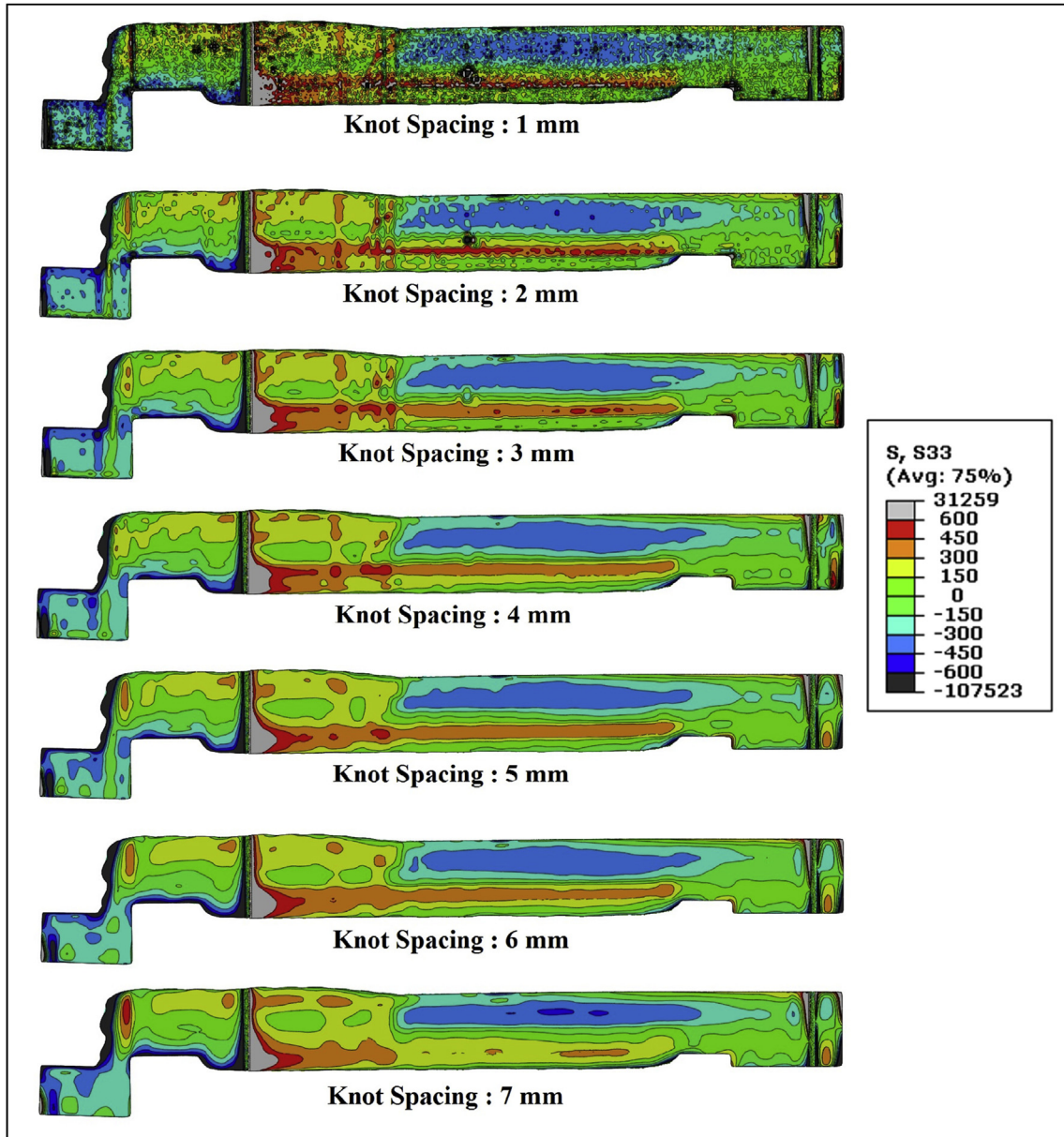
Fig. 10. Calculated stresses in the AW sample for surfaces fitted with different knot spacings.
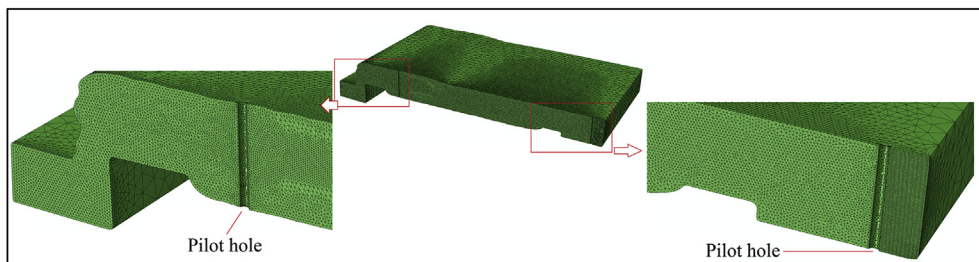

Fig. 11. The 3D half part created in Abaqus with a tetrahedral quadratic element mesh.

relaxation associated with the incremental drilling of a small hole, in this case with a diameter of 4 mm and depth of 2 mm. The strains were evaluated using a strain gauge rosette after each depth increment (fourteen increments for each hole) and the residual stresses were then calculated by employing equations which are summarised ASTM: E837 [23].

2.4. Hardness testing

Hardness testing was carried out to verify the effectiveness of
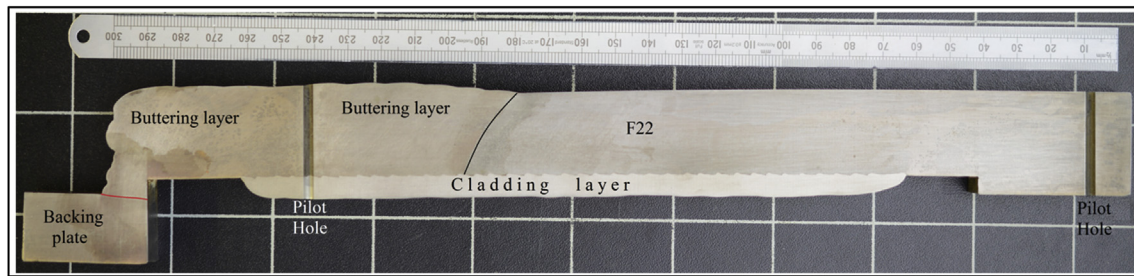
Fig. 12. Macrograph of the cut surface, aligned with the measured part outline, showing chosen material boundaries (the cladding overlay/F22 steel boundary is visible, whereas the boundary between the F22 steel/buttering layer is highlighted using a black line, while the boundary between the buttering layer and the backing plate is highlighted by a red line). (For interpretation of the references to colour in this figure legend, the reader is referred to the web version of this article.)

Fig. 13. Residual stress measurements made by incremental hole drilling in the buttering layer (a) and in the cladding overlay (b).

the PWHT operation, which in practice is supposed to reduce the material hardness to values below a threshold (i.e. 250 HV for steels [24]). Both the AW and PWHT samples were sectioned by EDM to produce specimens suitable for hardness measurements. The hardness measurements were made on a Struers Durascan 80 Automatic Hardness Testing Machine using a Vickers indenter with a 0.5 kg load, with a dwell period of 15 s. Measurements were made at 800 points in total, which were arranged along lines traversing the buttering-F22 interface, and along lines traversing the interface with the cladding overlay, over an area measuring 40 mm by 30 mm, with a maximum spacing between points of 1 mm.

3. Results and discussion

The residual stresses measured by the contour method are shown in Fig. 14 for the AW sample. The stresses are well resolved in an important area of interest (i.e. at the interface between the buttering layer, the F22 steel and the cladding overlay). The stresses in the buttering layer are tensile over a large region (due to the thermal contraction of a large number of weld beads), and in places they approach the level of the yield stress for the buttering material (~540 MPa). The bulk of the parent material is in compression, which acts to balance stress overall, although at the boundary with the buttering layer, and throughout the HAZ, the stresses are tensile and approach the yield stress in magnitude (~600 MPa). The cladding operation took place after buttering and, although the tensile stresses across large regions of the buttering layer are in the range between 150 and 400 MPa, they are higher at the interface between the buttering layer and the cladding overlay. Indeed, a region of high tensile stress (450–600 MPa) exists along the boundary between the cladding overlay and the associated HAZ in the buttering and parent materials.

It is likely that the magnitude of the tensile stresses in the

buttering layer as a whole were reduced to some extent by the deposition of the cladding overlay, since the thermal contraction that would have taken place in the cladding layer and adjacent HAZ will have acted to compress the adjacent materials (i.e. the F22 steel substrate and the buttering layer) in order to maintain compatibility in strain. The cladding overlay also appears to be sustaining low levels of tensile stress, with stresses decaying to zero near the surface of the overlay. It should be borne in mind that the cladding overlay was deposited in two layers and, using the same argument again, it is possible that the thermal contraction that took place in the second layer of cladding acted to reduce the tensile nature of stresses that would have been present in the first layer to be deposited. Unfortunately, it is not immediately obvious as to why the peak tensile stresses might arise in the vicinity of the HAZ associated with the deposition of the cladding overlay. The thermal expansion coefficients for ferritic steel and Inconel 625 are similar, and solid-state phase transformations would normally lead to a reduction in the tensile nature of residual stresses [25]. However, the presence of peak tensile stresses immediately under an overlay have also been reported by other researchers, for cases involving the deposition of austenitic stainless steels on to ferritic steels [26,27].

It can be seen that, in the vicinity of the pilot hole that passes through the buttering layer, grey areas appear in the coloured contour maps. These regions correspond to estimated stresses that are well in excess of the yield stress and, as such, they were deemed to be unrealistic and most likely artefacts resulting from localised plasticity during cutting. Such grey areas tended to arise at the entry and exit points for contour cuts, where cutting induced plasticity errors are most likely to occur [28–30]. An examination of the residual stresses in the buttering layer, and away from the interface with the cladding overlay in particular, reveals that the tensile nature of the residual stresses was generally similar on
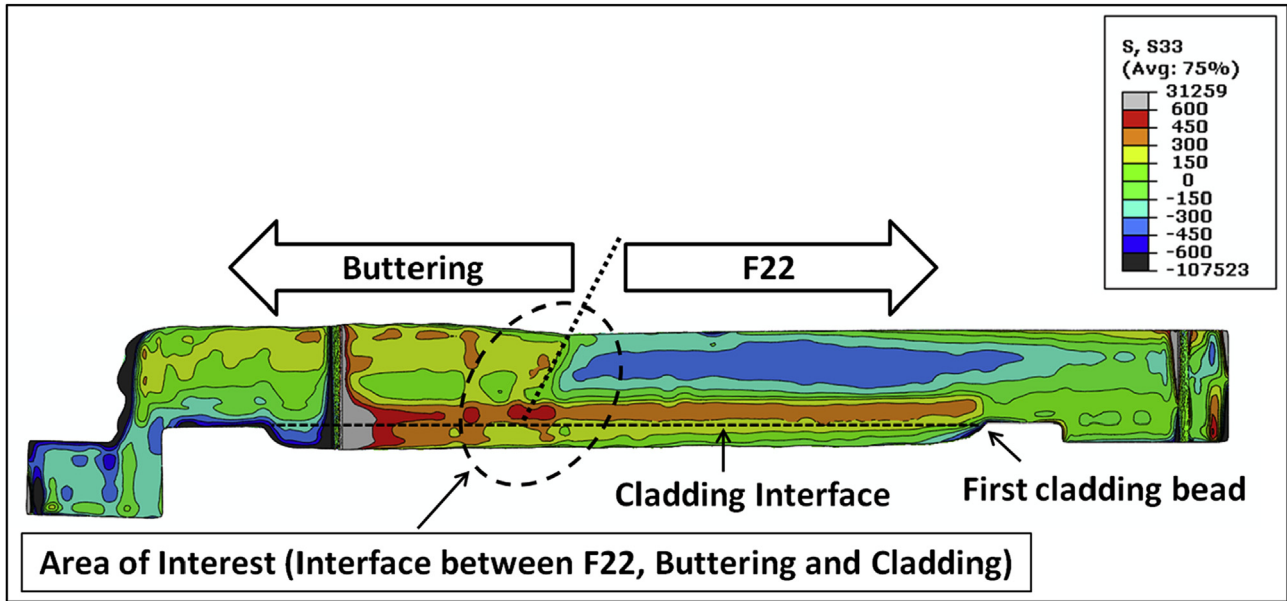
Fig. 14. Residual stresses acting in a direction normal to the cut surface in the AW sample, in MPa (grey areas indicate the estimated stresses are in excess of the yield stress).

either side of the pilot hole. In the vicinity of the cladding layer, however, there is a sudden reversal in the sign of the residual stresses moving from one side of the pilot hole to the other. Such an abrupt change in the sign of the residual stresses is difficult to rationalise based on an understanding of the welding process and resulting material behaviour. For this reason, the authors are of the view that the highly compressive stresses in the small portion of the cladding overlay that appears to the left of the pilot hole in Fig. 14 are also an artefact arising from cutting induced plasticity errors. Nevertheless, the vast majority of the residual stress map presented in Fig. 14 appears to be plausible.

In the PWHT sample (Fig. 15) the stresses were greatly reduced throughout, with the bulk of the buttering layer sustaining low levels of tension and the bulk of the parent material sustaining low levels of compression, with maximum magnitudes being in the order of 150 MPa in both cases. The cladding was also subject to low levels of tension, with maximum stresses having a similar magnitude. The PWHT operation can therefore be seen to have been effective, given that the peak stresses that were seen in the AW specimen (~600 MPa) have been reduced to a value closer to 150 MPa.

Line plots of residual stress were extracted for the samples in both the AW and PWHT conditions, and the locations at which they were extracted are shown in Fig. 16a and Fig. 16b. The line plots corresponding to each of the three locations are shown in Figs. 16c, d and e. For those regions that sustained highly tensile stresses in the AW sample, typical reductions in stress were in the order of ~300 MPa. After PWHT, the peak tensile stresses were less than
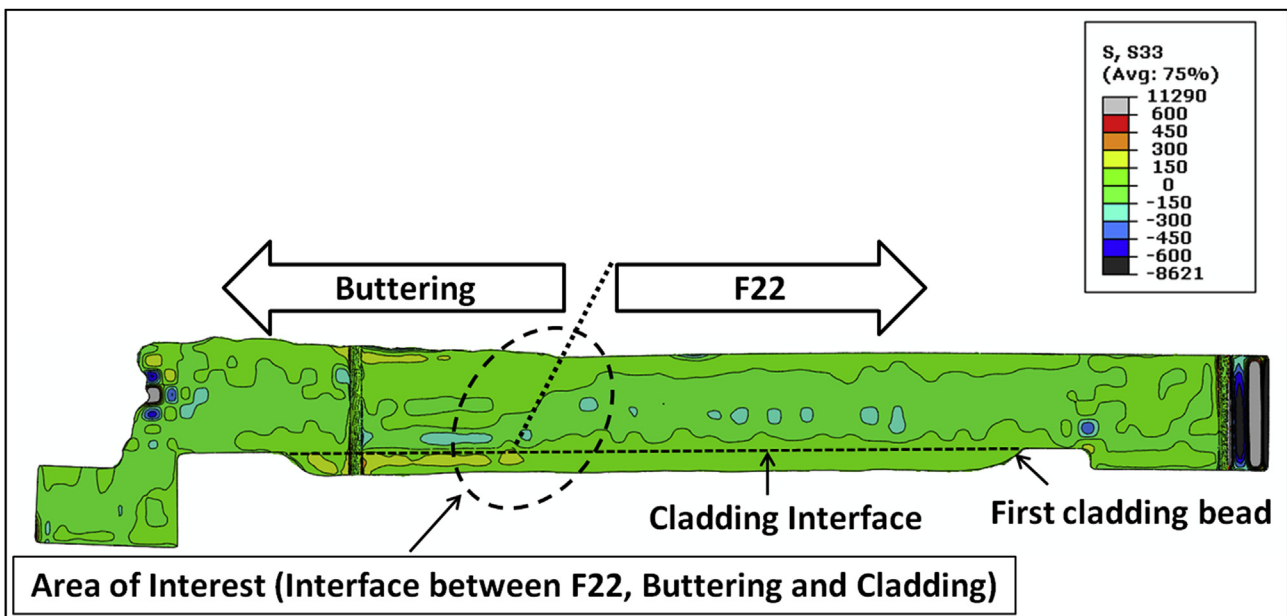

Fig. 15. Residual stresses acting in a direction normal to the cut surface in the PWHT sample, in MPa (grey areas indicate that the estimated stresses are in excess of the yield stress).
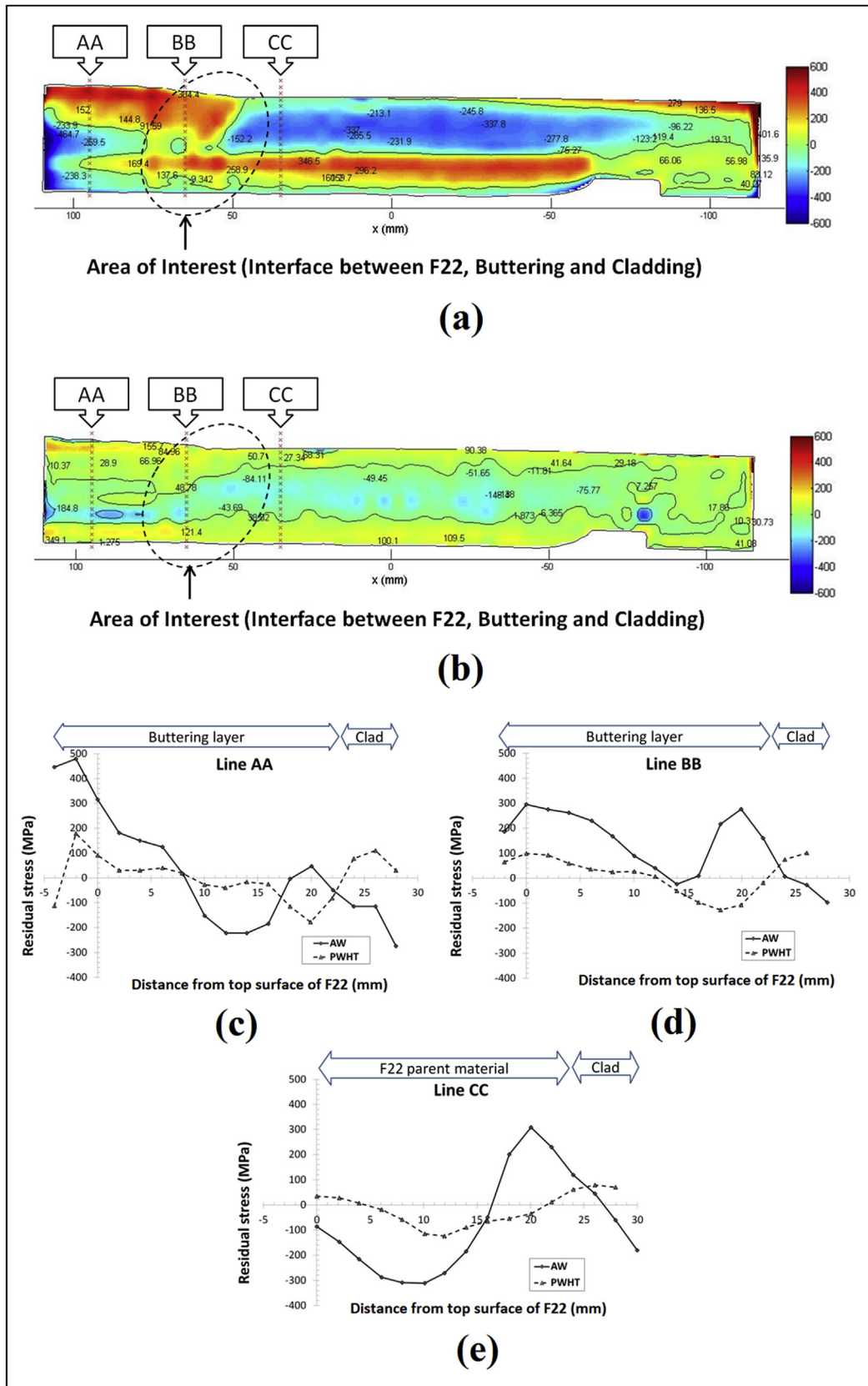
Fig. 16. Residual stress maps for (a) AW sample and (b) PWHT sample. The same stresses have been presented in the form of line plots as a function of depth at three locations (c–e).
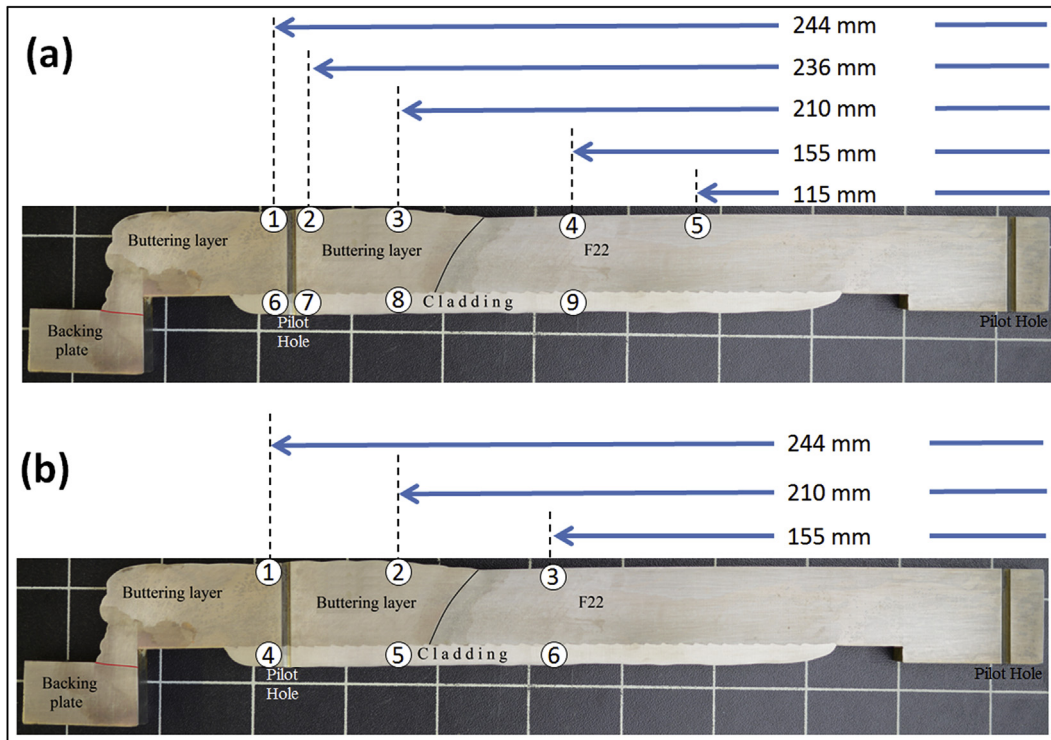
Fig. 17. The locations at which incremental hole drilling was carried out on the AW sample (a) and the PWHT sample (b).

200 MPa.

The locations at which the incremental hole drilling technique was applied are shown in Fig. 17. There were nine measurement locations in the AW sample and six in the PWHT sample. Locations #1 and #2 were on the top surface of the AW sample and on either side of the pilot hole. Locations #6 and #7 were also adjacent to the pilot hole in the AW sample but on the bottom surface, where the dominant influence on residual stresses will have been the cladding overlay. Locations #3 and #8 in the AW sample, as well as Locations #2 and #5 in the PWHT sample, were close to an area of interest which was in the immediate vicinity of the boundary between the F22 steel, the buttering layer and the cladding overlay. Location #9 in the AW sample and Location #6 in the PWHT sample were selected to evaluate the residual stresses in the cladding overlay but in a region not influenced by the buttering layer. Finally, Locations #3 - #5 were chosen to evaluate the residual stresses in the base material (F22 steel) in the PWHT and AW samples, respectively.

The hole drilling results are shown in Fig. 18 and Fig. 19 for the AW and PWHT samples, respectively. The vertical red dotted lines each comprise fourteen points, which correspond to residual stress measurements at fourteen different depths within an individual hole. The incremental hole drilling data span a range in depth from 0 to 2 mm, while the data extracted from the contour method measurements, which are represented by the blue lines in Figs. 18 and 19, correspond to residual stresses measured at a depth of 1 mm.

An examination of the data in Figs. 18 and 19 reveals that there is disagreement between the measurement techniques in the vicinity of the pilot hole, especially on the bottom surface of the specimens (e.g. at locations #6 and #7 in Fig. 18), which corresponds to the location of the cladding overlay. However, the agreement is somewhat better in the vicinity of the same pilot hole on the top surface (i.e. at locations #1, #2 and #3), with both measurement techniques indicating that the residual stresses are tensile.
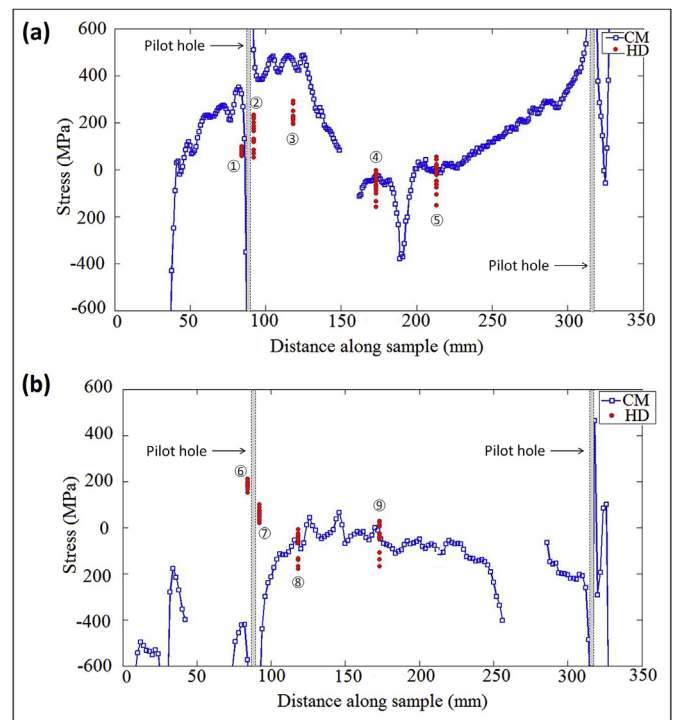

Fig. 18. Comparison between the longitudinal residual stresses measured by incremental hole drilling and by the contour method, for the AW sample (a: Top surface; b: bottom surface).

Furthermore, very good agreement is generally observed at other locations, including at #4, #5, #8 and #9 in the AW sample, and at locations #2, #3 and #6 in the PWHT sample. The fact that good
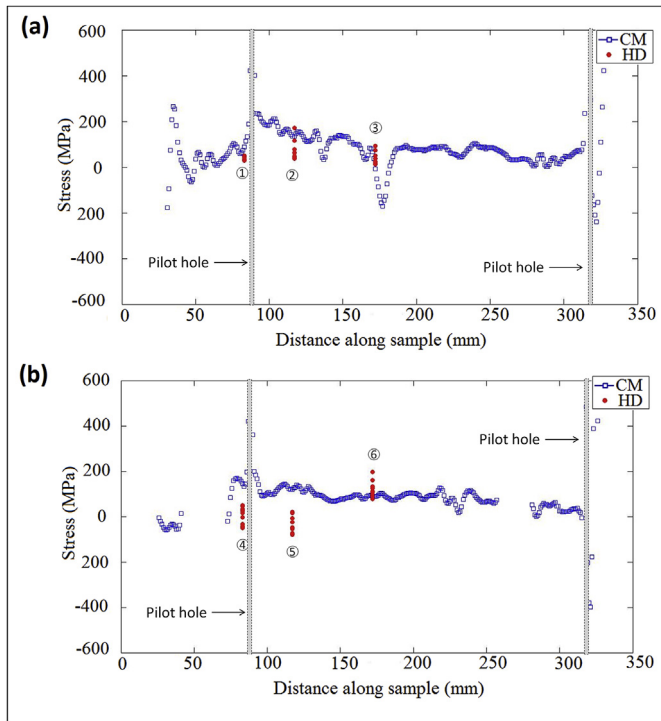
Fig. 19. Comparison between the longitudinal residual stresses measured by incremental hole drilling and by the contour method, for the PWHT sample (a: Top surface; b: bottom surface).

agreement is achieved at locations away from the pilot hole is reassuring, and it would suggest that the main features of the residual stress distributions, as obtained with the contour method measurements, are likely to be sound. The location where disagreement is most noticeable corresponds to the cladding overlay in the vicinity of the pilot hole. The contour method measurements suggest that the stresses in the cladding overlay generally remain similar at locations away from the pilot hole, but that

they change dramatically in the vicinity of the pilot hole, becoming highly compressive. In contrast, the incremental hole drilling results suggest a less dramatic change, with the stresses becoming moderately tensile. The authors are of the view that there is no physical basis for explaining a dramatic spike in compressive stress in the vicinity of the pilot hole and, on this basis, we believe that the compressive stresses that appear in this location in the contour method measurements are artefacts resulting from plasticity errors.

The contour method is only able to measure the residual stresses that act in a direction that is normal to the plane of the cut. In this work, the contour method was used to evaluate the longitudinal stresses in the weld mock-ups, and the results were compared to the stresses that were obtained with incremental hole drilling, as has been discussed above. However, the incremental hole drilling technique provides information on the stresses that act within near-surface planes that are normal to the drilling axis. As such, the incremental hole drilling technique could also provide an indication of the transverse residual stresses.

The transverse residual stresses that were measured are shown in Fig. 20 and Fig. 21 for the AW and PWHT specimens, respectively. A comparison between these two figures clearly reveals the extent to which the transverse residual stresses were relieved by the PWHT operation. A direct comparison is also provided in Fig. 22 for a specific location (i.e. Location #4 in the AW sample, which is equivalent to Location #3 in the PWHT sample), which reveals a drop in stress of ~180 MPa owing to PWHT.

The results in Fig. 23 confirm a dramatic reduction in hardness after PWHT. In the AW sample, the maximum hardness occurred in the HAZ within the F22 steel, being in the region of 400 HV, while in the majority of the specimen the hardness was ~250 HV. After PWHT the maximum hardness was ~290 HV at a small number of locations within the HAZ of the F22 steel, with the majority of the HAZ being at or below 250 HV. The hardness in the cladding overlay was 250 HV or lower, and the hardness in the majority of the buttering layer and the parent material was ~200 HV. This shows that PWHT has been effective in reducing the hardness to below 250 HV [24], with the exception of a few locations within the HAZ in the F22 steel.
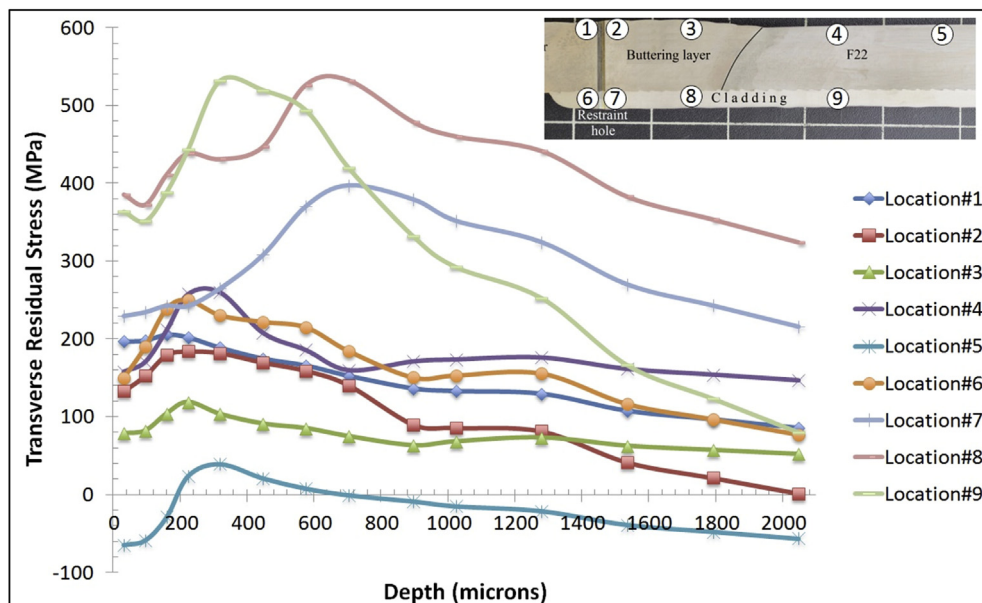

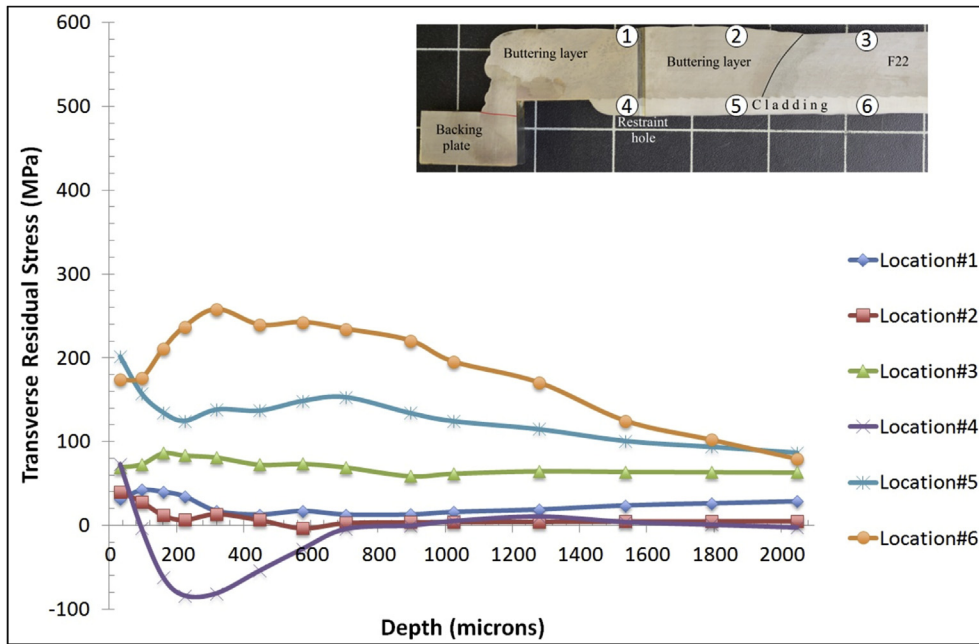**Fig. 20.** Distribution of transverse residual stresses at different depths in the AW sample.

Fig. 21. Distribution of transverse residual stresses at different depths in the PWHT sample.
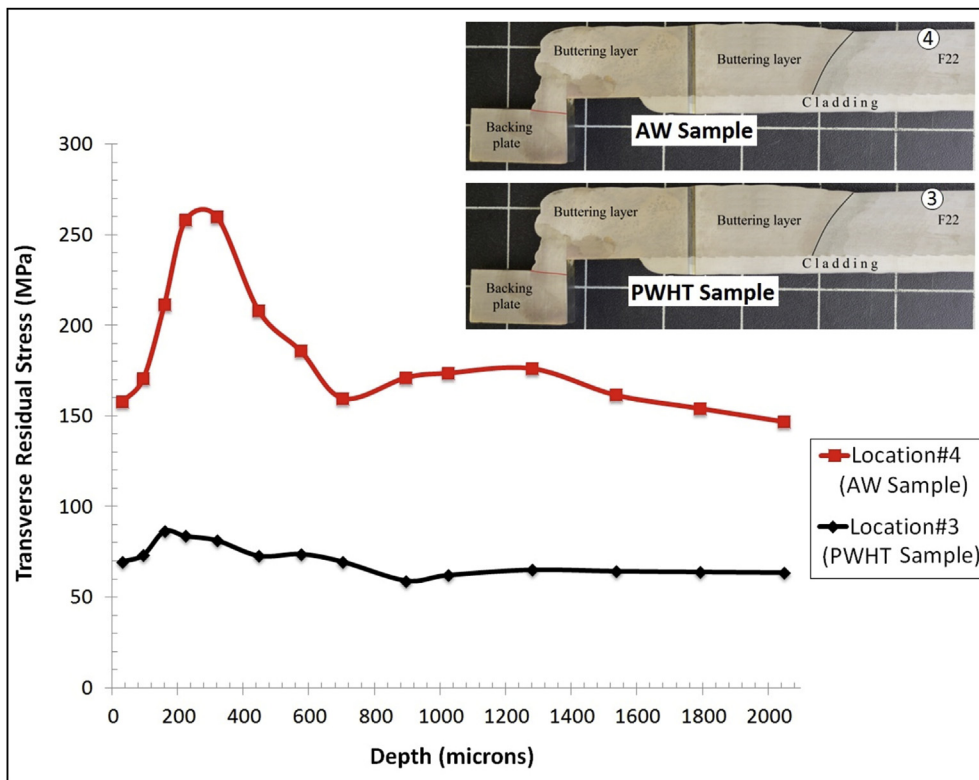

Fig. 22. Comparison between the transverse residual stresses in the AW sample (at Location #4) with those in the PWHT sample (at Location #3).

A comparison between the hardness maps that were obtained from each specimen and the corresponding residual stresses (as measured by the contour method) is shown in Fig. 24, for the region containing the interfaces between the F22 steel, the buttering layer and the cladding overlay. In the as-welded condition, it can be seen that there is a region subject to peak tensile stresses at the point where all three materials meet, and that this region is also subject to a high hardness. However, the peak in tensile stresses is effectively reduced by the PWHT operation, and the hardness is also much lower after PWHT, so any concerns from a structural integrity standpoint should be largely ameliorated by the PWHT operation. Nevertheless, it should be borne in mind that if for any reason PWHT were to be ineffective, then the region in the vicinity of where the F22 steel, the buttering layer and the cladding overlay all
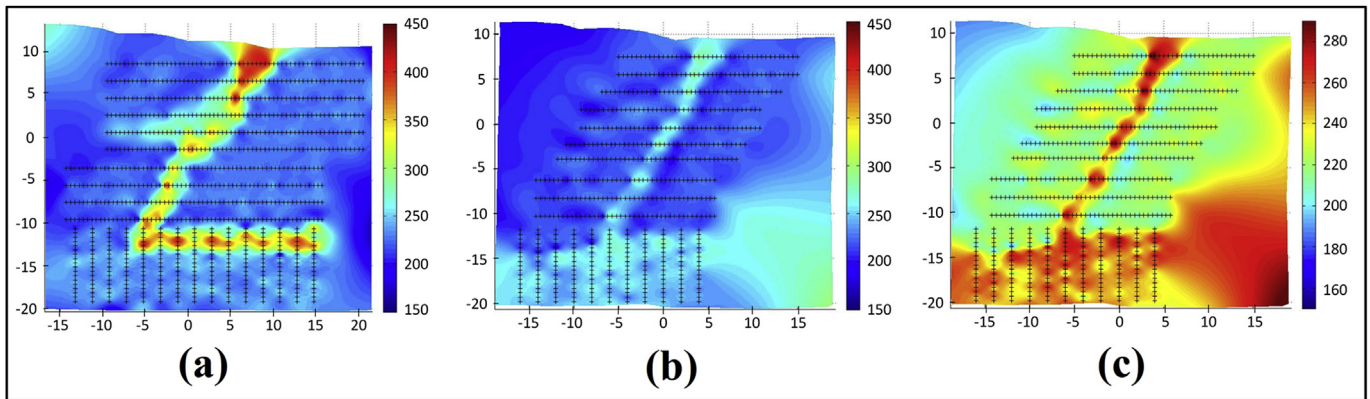
Fig. 23. HV$_{0.5}$ hardness maps for (a) the AW sample, (b) the PWHT sample using the same scale as for the AW sample and (c) the PWHT sample using a higher resolution (black crosses represent measurement locations).
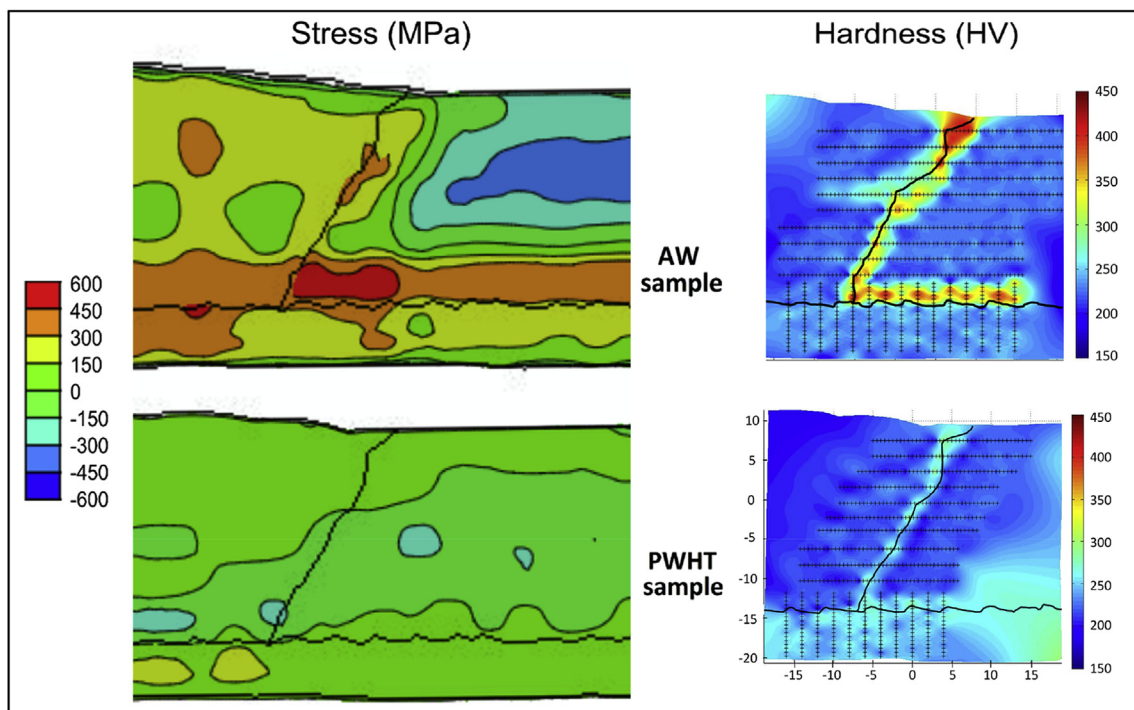

Fig. 24. A comparison between the hardness maps and the residual stress distributions as measured by the contour method. The peak in tensile stress that occurs at the interface between the F22 steel, the buttering layer and the cladding overlay is effectively relieved by PWHT, but the same region is still subject to moderately elevated hardness after PWHT.

meet will potentially be subject to accelerated degradation in service or premature failure.

4. Conclusions

The evolution of welding residual stresses during the buttering, cladding and PWHT processes in dissimilar metal welding was investigated in this study. Weld mock-ups were designed in such a way that enabled the manufacturing steps associated with a dissimilar metal weld to be replicated, albeit with a flat plate configuration as opposed to a pipe. This enabled the contour method to be applied for the purpose of generating two-dimensional residual stress maps across the dissimilar metal weld, producing results that seem plausible and which are generally compatible with those that were obtained close to the surface of the specimens with the incremental hole drilling technique. This work has produced a breadth of residual stress measurements that can be used to validate a computational framework for predicting residual stresses in dissimilar metal welds having different geometries (e.g. nozzle to pipe welds). The present work has generated the following conclusions:

1) The buttering process leads to the generation of tensile residual stresses throughout the buttering layer and the associated HAZ, which falls within the parent plate. While it is likely that subsequent cladding operations lead to a reduction in the magnitude of these tensile residual stresses, residual stresses in the range between 150 and 400 MPa were found to persist in the buttering layer after the cladding operation was completed.
2) The cladding process leads to the generation of a region of high tensile stresses immediately adjacent to the cladding overlay, in

the HAZ for the overlay. These stresses are in the order of the yield stress for the substrate material.

3) Very high tensile stresses were generated in the vicinity of the interface between the parent material, the buttering layer and the cladding overlay. This location also coincides with microstructures that have a high hardness in the as-welded condition.

4) PWHT is effective at reducing the tensile longitudinal and transverse residual stresses across the component, notwithstanding the presence of dissimilar materials across the joint. The hardness is also reduced significantly by PWHT, although in some regions within the HAZ the hardness was approaching 300 HV even after PWHT. This could raise concerns with respect to ensuring that structural integrity is maintained on real components with dissimilar metal welds of this type.

5) Further research is needed to establish best practice for the use of pilot holes in contour method measurements. In this work, a non-standard location was used in order to avoid excessive distortion of the test piece during cutting for the contour method measurements. However, the authors believe that the residual stress community would benefit from further guidance on the principles that might determine the optimum locations for pilot holes.

Acknowledgements

References

[1] Francis JA, Bhadeshia HKDH, Withers PJ. Welding residual stresses in ferritic power plant steels. Mater Sci Technol 2007;23:1009–20.

[2] Nelson TW, Lippold JC, Mills MJ. Investigation of boundaries and structures in dissimilar metal welds. Sci Technol Weld Join 1998;3:249–55.

[3] A. Blouin, S. Chapuliot, S. Marie, Dissimilar Metal Welds: Impact of the Residual Stresses on the Risk of Failure, ASME 2016 Pressure Vessels and Piping Conference, Vancouver, British Columbia, Canada (2016).

[4] D. Bremberg, J. Gunnars, E. Bonnaud, L.O. Edling, E. Kingston, RESIDUAL STRESSES IN ALLOY 182 PWHT BUTTERING AND ATTACHMENT - WELD VALIDATION BY MODELING AND MEASUREMENTS OF A FULL SCALE MOCKUP, Asme Pressure Vessels and Piping Conference - 2014, Vol 6b (2014).

[5] N. Yanagida, EFFECTS OF PIPE DIMENSIONS AND OUTER SURFACE-BUTTERING WELD CONDITIONS ON RESIDUAL STRESS DISTRIBUTIONS, Proceedings of the Asme Pressure Vessels and Piping Conference - 2008, Vol 6 Pt a and B (2009) 415–424.

[6] D.S. Swanek, J.R. MacKay, S.P. Farrell, R. Link, C.M.J. Timms, EFFECTIVENESS OF WELD BUTTERING REPAIR OF EXTERNALLY LOADED PRESSURE VESSELS WITH CORROSION DAMAGE, Proceedings of the Asme Pressure Vessels and Piping Conference - 2013, Materials and Fabrication, Vol 6b (2014).

[7] K. Serasli, H. Coules, D. Smith, Residual Stresses in Clad Nuclear Reactor Pressure Vessel Steels: Prediction, Measurement and Reconstruction, Asme Pressure Vessels and Piping Conference - 2015, Vol 6b (2015).

[8] J. Kusnick, M. Kirk, B.R. Bass, P. Williams, T. Dickson, EFFECT OF CLADDING RESIDUAL STRESS MODELING TECHNIQUE ON SHALLOW FLAW STRESS INTENSITY FACTOR IN A REACTOR PRESSURE VESSEL, Asme Pressure Vessels and Piping Conference - 2015, Vol 6a (2015).

[9] J. Jiang, G. Lian, M. Xu, C. Li, B. Chen, B. Li, Influence of Preheating Temperature on Mechanical Properties of Laser Cladding Layer, ASME 2016 11th International Manufacturing Science and Engineering ConferenceBlacksburg, Virginia, USA (2016).

[10] Dodge MF, Dong HB, Milititsky M, Barnett RR, Marques VF, Gittos MF. Asme, environment-induced cracking in weld joints in subsea oil and gas systems - part I. 2012.

[11] M.F. Dodge, H.B. Dong, M. Milititsky, R.R. Barnett, M.F. Gittos, Asme, ENVIRONMENT-INDUCED CRACKING IN WELD JOINTS IN SUBSEA OIL AND GAS SYSTEMS - PART II, Proceedings of the Asme 32nd International Conference on Ocean, Offshore and Arctic Engineering - 2013, Vol 3 (2013).

[12] Javadi Y, Najafabadi MA. Comparison between contact and immersion ultrasonic method to evaluate welding residual stresses of dissimilar joints. Mater Des 2013;47:473–82.

[13] N. Nazemi, J. Urbanic, A Finite Element Analysis for Thermal Analysis of Laser Cladding of Mild Steel With P420 Steel Powder, ASME 2016 International Mechanical Engineering Congress and Exposition, Phoenix, Arizona, USA (2016).

[14] S. Paul, K. Ashraf, R. Singh, Asme, RESIDUAL STRESS MODELING OF POWDER INJECTION LASER SURFACE CLADDING FOR DIE REPAIR APPLICATIONS, Proceedings of the Asme 9th International Manufacturing Science and Engineering Conference, 2014, Vol 2 (2014).

[15] Prime MB. Cross-sectional mapping of residual stresses by measuring the surface contour after a cut. J Eng Mater Technology-Transactions Asme 2001;123:162–8.

[16] Law M, Luzin V, Kirstein O. Iop, Effects of cutting and specimen size on neutron measurement of residual stresses, International Conference on Neutron Scattering 2009. Knoxville, TN: Iop Publishing Ltd; 2009.

[17] Hosseinzadeh F, Bouchard PJ. Mapping multiple components of the residual stress tensor in a large P91 steel pipe girth weld using a single contour cut. Exp Mech 2013;53:171–81.

[18] R.J. Dennis, N.A. Leggatt, E.A. Kutarski, INVESTIGATION OF THE PERFORMANCE OF THE CONTOUR RESIDUAL STRESS MEASUREMENT METHOD WHEN APPLIED TO WELDED PIPE STRUCTURES, Proceedings of the Asme Pressure Vessels and Piping Conference, Vol 6 Pts a and B (2010) 457–467.

[19] Kartal ME, Kang YH, Korsunsky AM, Cocks ACF, Bouchard JP. The influence of welding procedure and plate geometry on residual stresses in thick components. Int J Solids Struct 2016;80:420–9.

[20] M.B. Prime, M.R. Hill, A.T. DeWald, R.J. Sebring, V.R. Dave, M.J. Cola, Residual stress mapping in welds using the contour method, Trends in Welding Research, Proceedings, (2003) 891–896.

[21] M.E. Kartal, Analytical solutions for determining residual stresses in two-dimensional domains using the contour method, Proceedings of the Royal Society a-Mathematical Physical and Engineering Sciences, 469 (2013).

[22] Kartal ME, Lijedahl CDM, Gungor S, Edwards L, Fitzpatrick ME. Determination of the profile of the complete residual stress tensor in a VPPA weld using the multi-axial contour method. Acta Mater 2008;56:4417–28.

[23] ASTM. Standard test method for determining residual stresses by the hole-drilling StrainGage method. 2013. p. 1–16. ASTM E837-13a, ASTM, West Conshohocken, PA, United States.

[24] N. International, Petroleum and natural gas industries-Materials for use in H2S-containing-Environments in oil and gas production, Part 1: general principles for selection of cracking-resistant materials, (2001).

[25] Schnier G, Wood J, Galloway A. An experimental validation of residual stresses in weld clad pipelines. In: Zingoni A, editor. 5th international conference on structural engineering, mechanics and computation; 2013. p. 613–7. SEMC 2013London, UK.

[26] Benghalia G, Wood J. Material and residual stress considerations associated with the autofrettage of weld clad components. Int J Press Vessels Pip 2016;139:146–58.

[27] Schnier G, Wood J, Galloway A. Investigating the effects of process variables on the residual stresses of weld and laser cladding. Residual Stress Ix 2014;996:481–7.

[28] Traore Y. Controlling plasticity in the contour method of residual stress measurement. UK: Open University; 2013.

[29] Y. Traore, P.J. Bouchard, J. Francis, F. Hosseinzadeh, A NOVEL CUTTING STRATEGY FOR REDUCING PLASTICITY INDUCED ERRORS IN RESIDUAL STRESS MEASUREMENTS MADE WITH THE CONTOUR METHOD, Proceedings of the Asme Pressure Vessels and Piping Conference, Pvp 2011, Vol 6 a and B (2012) 1201–1212.

[30] Kerr M, Prime MB, Swenson H, Buechler MA, Steinzig M, Clausen B, et al. Residual stress characterization in a dissimilar metal weld nuclear reactor piping system mock up. J Press Vessel Technology-Transactions Asme 2013;135.